Molecular Vision 2021; 27:666-678 <http://www.molvis.org/molvis/v27/666>
Received 2 April 2021 | Accepted 5 December 2021 | Published 7 December 2021

Collagen matrix perturbations in corneal stroma of Ossabaw mini pigs with type 2 diabetes

Nishant R. Sinha,[1,2] Praveen K. Balne,[1,2] Filiz Bunyak,[3] Alexandria C. Hofmann,[2] Rayne R. Lim,[4] Rajiv R. Mohan,[1,2,5] Shyam S. Chaurasia[2,6]

[1]Harry S. Truman Memorial Veterans' Hospital, Columbia, MO; [2]One-Health Vision Research Program, Departments of Ophthalmology and Biomedical Sciences, College of Veterinary Medicine, University of Missouri, Columbia, MO; [3]Department of Computer Science, University of Missouri, Columbia, MO; [4]Department of Ophthalmology, University of Washington, Seattle, WA; [5]Mason Eye Institute, School of Medicine, University of Missouri, Columbia, MO; [6]Department of Ophthalmology and Visual Sciences, The Eye Institute, Medical College of Wisconsin, Milwaukee, WI

Purpose: Diabetes mellitus (DM) is a metabolic disorder that affects over 450 million people worldwide. DM is characterized by hyperglycemia, causing severe systemic damage to the heart, kidneys, skin, vasculature, nerves, and eye. Type 2 diabetes (T2DM) constitutes 90% of clinical cases and is the most common cause of blindness in working adults. Also, about 70% of T2DM patients show corneal complications including delayed wound healing, often described as diabetic keratopathy (DK). Despite the increasing severity of DM, the research on DK is bleak. This study investigated cellular morphology and collagen matrix alterations of the diabetic and non-diabetic corneas collected from Ossabaw mini pigs, a T2DM animal model with a "thrifty genotype."

Methods: Pig corneas were collected from six-month-old Ossabaw miniature pigs fed on a western diet (WD) for ten weeks. The tissues were processed for immunohistochemistry and analyzed using hematoxylin and eosin staining, Mason Trichrome staining, Picrosirus Red staining, Collage I staining, and TUNEL assay. mRNA was prepared to quantify fibrotic gene expression using quantitative reverse-transcriptase PCR (qRT-PCR). Transmission electron microscopy (TEM) was performed to evaluate stromal fibril arrangements to compare collagen dynamics in WD *vs.* standard diet (SD) fed Ossabaw pig corneas.

Results: Ossabaw mini pigs fed on a WD for 10 weeks exhibit classic symptoms of metabolic syndrome and hyperglycemia seen in T2DM patients. We observed significant disarray in cornea stromal collagen matrix in Ossabaw mini pigs fed on WD compared to the age-matched mini pigs fed on a standard chow diet using Masson Trichome and Picrosirius Red staining. Furthermore, ultrastructure evaluation using TEM showed alterations in stromal collagen fibril size and organization in diabetic corneas compared to healthy age-matched corneas. These changes were accompanied by significantly decreased levels of Collagen IV and increased expression of matrix metallopeptidase 9 in WD-fed pigs.

Conclusions: This pilot study indicates that Ossabaw mini pigs fed on WD showed collagen disarray and altered gene expression involved in wound healing, suggesting that corneal stromal collagens are vulnerable to diabetic conditions.

Diabetes mellitus (DM) is a metabolic disorder characterized by chronic hyperglycemia that affects multiple organs including the eye. DM has reached epidemic proportions in the last decade and has become a leading risk factor for blindness globally [1,2]. Out of the two hyperglycemic insults, Type I DM (T1DM) is caused by an autoimmune response to pancreatic islet cells, causing a defect in insulin production and secretion, while Type II DM (T2DM) is more prevalent and caused by a defect in the insulin receptor function, causing a gradual decline in insulin production [3,4]. Irrespective of the DM types, the most severe ocular complication is diabetic retinopathy (DR)—a retinal microvascular disorder in working adults [2,5-7]. Besides the retinal damage, DM causes complications in the cornea, which are commonly referred to as diabetic keratopathy (DK). Between 45 and 70% of diabetic patients have shown corneal complications [8]. Despite the increasing clinical cases with severe DK pathologies, research in DM-related corneal complications is meager.

Recent clinical studies documenting ocular surface status during eye exams in diabetic patients describe significant alterations in the tear film, conjunctiva, corneal epithelial cells, nerves (corneal neuropathy), stroma, endothelial cells, and corneal biomechanics [9-11]. Further studies have shown that diabetic corneas are more susceptible than normal corneas to bacterial and viral infections [12-14]. Currently, one-fourth of corneas harvested for transplants in the United States are from Diabetic donors [10,11], which may present a significant risk to graft recipients and cause more frequent post-surgical complications [15–17].

Correspondence to: Shyam S. Chaurasia, Department of Ophthalmology and Visual Sciences, The Eye Institute, Medical College of Wisconsin, 925 N 87th Street, Milwaukee, WI 53226-0509; email: schaurasia@mcw.edu

Previous studies have focused on changes in the corneal epithelium, nerves, and endothelium [8,9,12,15,16]. However, studies investigating the effects of diabetes on the corneal stroma are limited to the reduction of keratocyte density [18]. Advanced glycation endproducts accumulation induces changes in metabolic and lipidomic pathways [19]. As per the literature, this phenomenon also causes increased central corneal thickness and rigidity [20,21]. Nevertheless, the effects of high glycation endproducts accumulation on diabetic cornea remain poorly understood. Collagens are crucial in maintaining corneal shape and size. Structurally, abnormal collagen fibril bundles have been reported in the diabetic corneas of human and monkey T1DM models [22,23]. The stroma constitutes the bulk of the cornea and contains lamellae of collagen-rich connective tissue embedded into proteoglycan bed and keratocytes. The collagen lamellae are characterized by fibrils' distinctive features, narrow with uniform diameter and arranged with a high degree of lateral ordering, and define the cornea's optical and tensile biomechanical properties [3]. The predominant collagens in the cornea are types I, III, V, VI, and XIII.

Cornea is a unique tissue because of the distinctive collagen fibril arrangement, shape, cellular, and optical properties that collectively render two-third of refraction (vision) to the eye. Previous studies in non-ocular tissues have suggested that diabetes negatively impacts collagen fibrils [24-29]. Saito et al. showed that DM causes deterioration of bone quality with a significantly different distribution of collagen spacing in diabetic rats than in non-diabetic controls [30]. Interestingly, they noted very little change in bone mass and bone mineral density. These reports prompted us to test the hypothesis that DM affects the collagen distribution and arrangement in the stroma and alters normal wound healing parameters in the cornea using a T2DM Ossabaw mini pig model. Ossabaw mini pigs are breeds of wild boar that survived the harsh conditions on Ossabaw Island, Georgia, United States [31] and adopted a "thrifty genotype." Ossabaw mini pigs develop hyperglycemia and classical metabolic syndrome (MetS) features when fed on WD [32]. Recently, our laboratory described the hallmarks of hyperglycemia and hyperlipidemia alongside retinal neurodegenerative and microvascular changes in these mini pigs [33]. Many studies have shown a direct correlation between DR and DK [9,34], making Ossabaw mini pigs an ideal model for studying T2DM induced collagen fibrils in the corneal stroma. This pilot study is an extension of our previous study [33] to examine changes in cellular morphology and collagen matrix in the corneas of diabetic and non-diabetic Ossabaw mini pigs.

METHODS

Animals: All experimental procedures were approved by the Institutional Animal Care and Use Committee, University of Missouri Columbia, and adhered to the ARVO Statement for the Use of Animals in Ophthalmic and Vision Research. Adolescent female and male Ossabaw mini pigs (RRID:NSRRC:0008) were housed at the Animal Science Research Center, the University of Missouri, Columbia, MO, in a temperature-controlled environment with 12 h light and 12 h dark cycle. Following weaning, all pigs were fed on a standard commercially available chow diet (catalog no. 5L80, Lab Diet; 3.03 kcal/g, 71% from carbohydrate, 18.5% from protein, and 10.5% from fat) until 3.5 months of age. Twelve male and female mini pigs were divided into two groups equally and fed on SD and WD for ten weeks. SD mini pigs were kept on the standard chow, while pigs in the WD group were fed a high-fat/high-fructose corn syrup/high-calorie diet (5B4L, Lab Diet; 4.14 kcal/g, 40.8% from carbohydrate, 16.2% from protein, and 43% from fat). At six months of age, following a 20-h overnight fast, pigs were anesthetized (5 mg/kg of Telazol and 2.25 mg/ kg of xylazine mixture) and weighed (for body mass determination), blood was collected, and mini pigs were subsequently euthanized for tissue collection as described earlier [33]. Both retinal and corneal tissues were collected post-euthanasia in the study.

Ossabaw pig tissue collection: Following euthanasia, eyes were enucleated with surgical forceps and Westcott scissors. An incision was made at the ora ciliaris, approximately 5 mm posterior to the corneal limbus, using a number of 11 scalpel blade. A circumferential cut was made to remove the anterior ocular tissues, including the ciliary body and lens. The ciliary body, lens, and iris were removed from the cornea using surgical forceps and Westcott scissors under a dissecting surgical microscope (Leica Wild M690, Leica Microsystems Inc., Buffalo Grove, IL). The corneal tissues were placed in 1.5 ml Eppendorf tubes and stored at −80°C. Later, corneas were cut into three equal parts: one part was used for histology studies, and the other two parts were used for molecular studies and transmission electron microscopy (TEM) analysis. For histology, corneal tissue was immediately placed into molds containing an optimal cutting temperature (OCT) compound and snap-frozen in a container of 2-methyl butane immersed in liquid nitrogen. Frozen tissues were maintained at −80°C until sectioning and further evaluation. Tissues were sectioned at 8 µm thickness, mounted on microscopic glass slides (SuperFrost Plus, Fisher Scientific), and slides were preserved at −80°C for subsequent analysis.

Hematoxylin and Eosin (H&E) staining: H&E staining was performed following the standard technique [35]. Briefly, cryo-frozen corneal sections were incubated for 15–20 min at room temperature, washed in PBS for 10 min, and dipped in hematoxylin for 5 min, followed by a rinse in running DI water, one dip in 1% acid-alcohol, and 1 min in 0.3% ammonia water. The slides were incubated in 95% alcohol, followed by eosin. The tissues were then dehydrated in absolute alcohol, cleared in CitriSolv solution (Decon Laboratories, King of Prussia, PA), and finally mounted with cytoseal (Richard-Allan Scientific, Kalamazoo, MI). The images of H&E-stained tissues were captured with a bright-field microscope (Leica) equipped with a digital camera and imaging software (SpotCamRT KE; Diagnostic Instruments, Sterling Heights, MI).

Masson trichrome and picrosirus red staining: Eight-micron thick Ossabaw pig corneal tissue sections from the WD and SD groups were subjected to Masson's trichrome staining to evaluate the alterations in collagen, a primary component of extracellular matrix (ECM). Masson's trichrome and Picrosirus Red staining was performed by the Veterinary Medical Diagnostic Laboratory at the University of Columbia, MO, as described earlier [35].

Collagen I Immunohistochemistry: Eight-micron thick corneal sections were prepared, postfixed at room temperature for 10 min, and blocked with 5% donkey serum for 1 h at room temperature. Immunostaining was performed using collagen I (COL1) (1:200; Abcam), kept overnight at 4°C, and secondary stained with Alexa-Fluor 594 antibodies (1:500; Life Technologies) for 4 h. A drop of DAPI antifade Vectashield medium (H1200) was applied, and sections were mounted with premier coverslips (Thermo Fisher). (DAPI; Vector Laboratories) The stained sections were viewed and photographed with a fluorescence microscope (Leica DM 4000B, Leica Microsystems Inc., Buffalo Grove, IL) equipped with a digital camera (SpotCam RT KE, Diagnostic Instruments Inc., Sterling Heights, MI). Negative control samples were stained by excluding primary or secondary antibody in serially sectioned slides.

TUNEL assay: Keratocyte apoptosis in the corneas of the WD- and SD-fed mini pigs was determined by TUNEL assay (ApopTag; Millipore, Temecula, CA). Corneal sections were fixed in 1% PFA for 10 min, and a TUNEL assay was performed following the manufacturer's instructions, including suitable positive and negative controls. Rhodamine-conjugated apoptotic cells (red) and 40,6-diamidine-20 -phenylindole dihydrochloride (DAPI)–stained nuclei (blue) were viewed and photographed with a fluorescence microscope (Leica) fitted with a digital camera system (SpotCamRT KE; Diagnostic Instruments, Sterling Heights, MI). DAPI-stained nuclei and TUNEL-positive cells in untreated and treated tissues were quantified at 100x magnification in six randomly selected non-overlapping areas [36,37]. Negative control samples were stained by excluding the Tdt enzyme or Anti-Digoxigenin Conjugate in serially sectioned slides.

Transmission electron microscopy (TEM): The ciliary body, iris, and lens were removed as described. One-fourth of the cornea was placed in one milliliter of TEM primary fixative (2% paraformaldehyde, 2% glutaraldehyde in 100 mM sodium cacodylate buffer; pH 7.35). Tissues were then transitioned into acetone, infiltrated with Epon resin (250 W for 3 min), and polymerized at 60°C overnight. Corneas were cut transversely with an ultramicrotome to obtain 2 µm thick sections for histologic examination. The cornea was further trimmed to a length of 500 µm and cut with a diamond knife to yield 75 nm sections for TEM. Images were acquired with a JEOL JEM 1400 transmission electron microscope (JEOL USA Inc., Peabody, MA) at 80 kV on a Gatan Ultrascan 1000 CCD, at 20000x magnification.

For automated quantification of corneal collagen fibrils in TEM images, an in-house image processing and analysis software was developed as described in the previous study [38]. Briefly, the algorithm comprised three main modules, (i) fibril detection, (ii) shape analysis and cluster decomposition, and (iii) size and interfibrillar distance analysis. A multi-scale Hessian matrix was used to detect collagen fibrils. Hessian matrix (Equation 1) described the second-order structure of local intensity variations around each point of the image L (x, y), and eigenvalues $\lambda_{1,2}$ (Equation 2) of the Hessian matrix was used to detect blob-like, or ridge-like structures. Table 1 shows possible local orientation patterns based on the eigenvalues of the Hessian matrix.

$$Hessian_{\sigma}(X,Y) = \begin{bmatrix} L_{xx}(X,Y) & L_{xy}(X,Y) \\ L_{xy}(X,Y) & L_{yy}(X,Y) \end{bmatrix}$$

Table 1. Possible orientation patterns based on the value of eigenvalues λ 1, λ 2 of the Hessian matrix (|λ 1| ≥ | λ 2|).

1	2	Orientation pattern
Low	Low	Flat or noise no preferred direction
High -	Low	Bright tubular structure
High +	Low	Dark tubular structure
High -	High -	Bright blob-like structure
High +	High +	Dark blob-like structure

$$\lambda_{1,2} = \frac{1}{2}(L_{xx} + L_{yy} \pm \sqrt{(L_{xx} + L_{yy})^2 + (2L_{xy})^2})$$

Hessian matrix was computed by convolving the image with derivatives of the Gaussian kernel, where scale s represented the standard deviation of the Gaussian kernel and controlled the radius of the detected structures. A coarse fibril mask was produced by computing Hessian matrix and thresholding λ_1 (Hessian) as below (Equation 3):

$$Mask_{fibril}(X,Y) = \begin{Bmatrix} 1\lambda(Hessian(x,y) < \varepsilon \\ 0 \text{ otherwise} \end{Bmatrix}$$

The quantification of morphology and spatial organization of fibrils requires accurate identification and localization of individual fibrils. Hessian-based detection efficiently segmented regions occupied by fibrils from the background but failed to separate some neighboring fibrils and merge them into clusters. To identify individual fibrils, shape analysis and cluster decomposition module were developed based on previously reported modules [39,40]. Specifically, the first connected component labeling was applied to the detection mask and disconnected blobs. Then, to each detected blob B_i, an ellipse E_i was fitted. Blob and ellipse areas: area (B_i), area(E_i), and ratio r=area(E_i) - area(B_i))/area(B_i) were then computed. Each detected blob Bi was classified into one of the three classes (spurious detection, single fibril, or fibril cluster) using size and shape indices and their means and variances over the image. Blobs classified as spurious detection were removed; blobs classified as single fibril were kept intact. The marker-controlled watershed transformation was used to decompose fibril clusters into individual fibrils [41]. Regional maxima of distance transform were used as markers. To suppress spurious regional maxima and prevent over-segmentation, H-maxima transform was applied to the distance transform before detecting regional maxima [42].

The module then computed parameters concerning fibril morphology and spacing, such as fibril radius, fibril area fraction, and interfibrillar distance. From the refined segmentation, fibril centroids were computed. Delaunay triangulation and vertex coloring were applied to the located centroids, and a colored neighborhood graph was generated, as previously described [39,43]. In the neighborhood graph, nodes corresponded to individual fibrils, and edges linked immediate neighbors. For each node in this neighborhood graph, two specific neighbors were identified: the nearest immediate neighbor (red edges) and the farthest immediate neighbor (blue edges). A second graph (nearest/farthest neighborhood graph) was constructed using only these specific links. Fibril-to-fibril interactions were assessed, and the spatial organization of collagen fibrils were described using these two neighborhood graphs. Various descriptors from these graphs, such as mean and standard deviation, were then calculated as described previously [38].

Quantitative reverse transcriptase PCR (qRT-PCR): For molecular studies, corneal tissues were minced in a tissue lyser (TissueLyser LT, Qiagen) in RLT buffer (Qiagen, Valencia, CA), and total RNA was isolated using the RNeasy kit (Qiagen, Valencia, CA) following the manufacturer's instructions. The reverse transcriptase enzyme kit was used to synthesize first-strand cDNA (Promega, Madison, WI) [44]. The One Step Plus Real-Time PCR system (Applied Biosystems, Carlsbad, CA) was used for quantitative PCR (qPCR). A 20µl reaction mixture containing 2µl cDNA, 2µl forward and reverse primers (200nM each), and 10µl of 2X All-in-One PowerUp SYBR green master mix (Applied Biosystems) was run at a universal cycle (95°C for 10 min, 40 cycles at 95°C for 15 s, and 60°C for 60 s), as previously reported [44]. Forward and reverse gene-specific primer sequences are shown in Table 2. Glyceraldehyde 3-phosphate dehydrogenase (GAPDH) was used as an endogenous reference gene. The threshold cycle (Ct) was used to detect the increase in the signal associated with the exponential growth of PCR products during the log-linear phase. ΔCt for each sample was calculated by subtracting the Ct of the target gene from that of the Ct of the endogenous reference gene, and ΔΔCT was calculated by subtracting the ΔCt of the test sample from that of the ΔCt of the control sample. The relative mRNA expression was calculated using the 2-ΔΔCt method and reported as a relative fold change over the corresponding control values. The amplification efficiency for the qRT-PCR was similar for all templates used, and the difference between linear slopes was below 0.1. The qPCR was performed in triplicate for each sample, and a minimum of three independent experiments was conducted.

Statistical analysis: The GraphPad Prism 8.2.1 (GraphPad Software, La Jolla, CA) software was used for statistical analysis. Each experiment was conducted independently in triplicate, and the values were expressed as mean ± SEM. For statistical analysis, the Student *t*-test and two-way ANOVA with Bonferroni post hoc test were used. The value of $p \leq 0.05$ was considered as the significance level.

RESULTS

Ossabaw mini pigs fed on WD exhibits signs of T2DM: Ossabaw mini pigs fed on WD showed clinical signs of metabolic syndrome and hyperglycemia, demonstrating

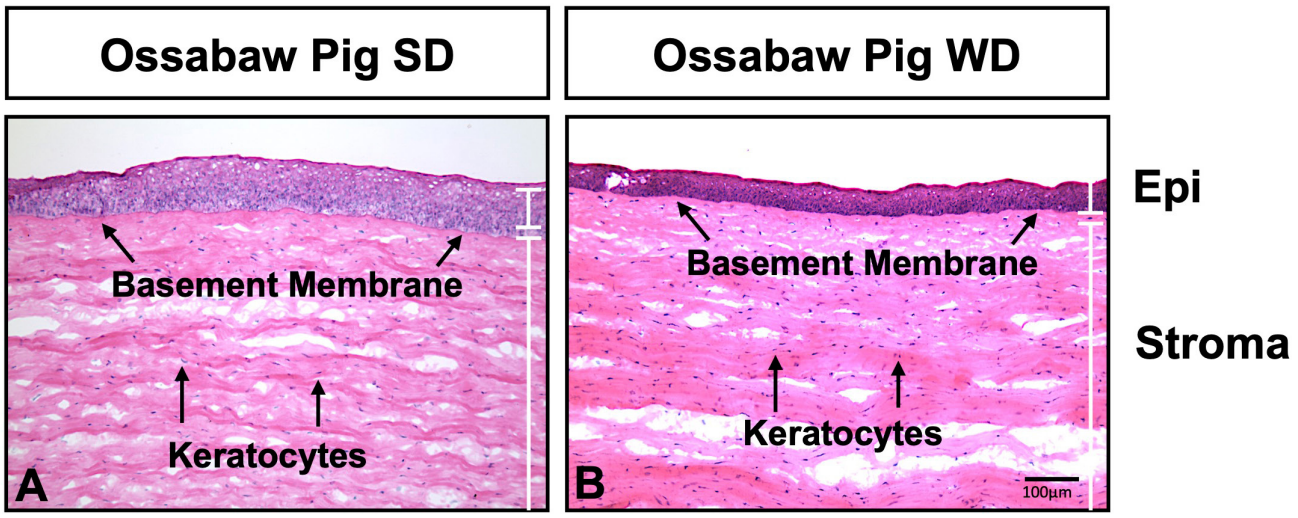

Figure 1. Hematoxylin and Eosin staining suggest an increase in keratocytes (black arrows) in the Western diet (WD) fed Ossabaw mini pigs (**B**) compared to the Standard diet (SD) fed pigs (**A**). Green arrows indicate the basement membrane.

characteristic features of T2DM. Ossabaw mini pigs showed a significant increase in body mass, cholesterol, dyslipidemia, and significantly high plasma glucose after 10 weeks on WD compared to the SD-fed pigs [33]. Additionally, WD-fed pigs showed elevated insulin resistance levels based on the Homeostatic Model Assessment of Insulin Resistance (HOMA-IR), a clinical indicator of insulin resistance described in our previous study [33].

Ossabaw mini pigs fed on WD displays increased activation and apoptosis of keratocytes: H&E staining in WD pig corneas showed intensified nuclei staining in the stroma (Figure 1B) compared to SD pigs (Figure 1A). TUNEL assay performed in the Ossabaw mini pigs suggested elevated apoptotic positive cells = red in WD corneal stroma (Figure 2B) compared to the SD group (Figure 2A). Total number of tunnel positive cells per field were considered for objective comparison between the two groups.

Ossabaw pigs fed on WD shows irregularity in the corneal stroma: We used Mason Trichome, a tricolor stain, which showed increased collagen (blue), reduced cytoplasm staining (pink/red), and increased cell nuclei (black) in WD pigs (Figure 3B) compared to SD pigs (Figure 3A). Immunohistochemistry staining of T2DM pig corneas with COL 1 displayed an irregular distribution of collagen fibrils in the WD pigs (Figure 4B) compared to SD pigs (Figure 4A). This observation was further confirmed with the use of Picrosirus Red staining, where Ossabaw pigs on a WD increased collagen staining (red) in the stroma (Figure 5B) compared to the SD control group (Figure 5A).

Ossabaw mini pigs fed on WD shows ultrastructural defects in stromal collagen matrix: Corneas were analyzed

Table 2. Real time primers used in the study.

S. No	Gene Name	Forward sequence (5′ – 3′)	Reverse sequence (3′ – 5′)
1	GAPDH	TGG GTG TGA ACC ATG AGA	GTC CTT CCA CGA TAC CAA AG
2	αSMA	TAC TCC GTC TGG ATT GGT	CTT CGT CGT ACT CCT GTT TG
3	FN	CAG CTC CGA GAT CAG TGC AT	TCC GAA TCC TGG CAT TGG TC
4	TGFβ1	GAA AGC GGC AAC CAA ATC	CGA GAG AGC AAT ACA GGT TC
5	TIMP1	GAC ATC CGG TTC ATC TAC AC	CAC AGT TGT CCA GCT ATG AG
6	COL IV	GAT AAG GGA GAT GTG GGT CT	TCC TTT CTC TCC TTG GTC TC
7	COL III	TGT GGC CCA GAA GAA CTG GTA CAT	ACT GGA ATC CAT CGG TCA TGC TCT
8	MMP I	AGT GAC TGG GAA ACC AGA TGC TGA	TCA GTG AGG ACA AAC TGA GCC ACA
9	MMP 9	ATT TCT GCC AGG ACC GCT TCT ACT	TTG TAT ACG GCA AAC TGG CTC CTT

ultrastructurally for the evaluation of stromal collagen fibril arrangements (Figure 6 and Figure 7). TEM showed marked alterations in stromal collagen fibril size and fibril organization. We used computer-generated collagen ellipses of transverse corneal TEM images (Figure 6). A significant change was noted in areas measured regarding the fibrils' frequency (p = 0.0034). Ossabaw mini pigs on WD had smaller-sized collagen fibers compared to the pigs on SD. SD mini pigs had a range of collagen fibers with two average sizes of approximately 300 pixels and 900 pixels. In contrast, WD mini pigs had a lower number of small fibers, and the average size of larger fibers decreased from 900 fibers to approx. 800. Adding to size differences, WD pigs had differences in the interfibrillar distance (IFD). Figure 7 describes a fibril graph connecting individual collagen fibrils with their neighbors. Further analysis on fibril distances was performed by mapping minimum (red lines) and maximum (blue lines) IFD. WD mini pigs showed statistically significant changes in minimum (p = 0.0212) and maximum (p = 0.0018) IFD compared to the SD group, indicating a perturbation in collagen distribution corneal stroma.

Ossabaw mini pigs fed on WD depicts altered gene expression related to collagen and fibrosis in the corneal stroma: Collagen-related gene expression also showed a significant decrease in collagen IV (COL4) expression and increased matrix metalloproteinase 9 (MMP9) expression in the WD diet-fed Ossabaw mini pigs compared to the SD diet-fed pigs. In contrast, Collagen III (COL3), MMP1, and Tissue Inhibitor of Metalloproteinase 1 (TIMP1) showed no change in the gene transcripts (Figure 8A). We also studied the expression of fibrosis-related genes in the pig corneal stroma. Alpha-Smooth muscle actin (αSMA) and fibronectin (FN) showed

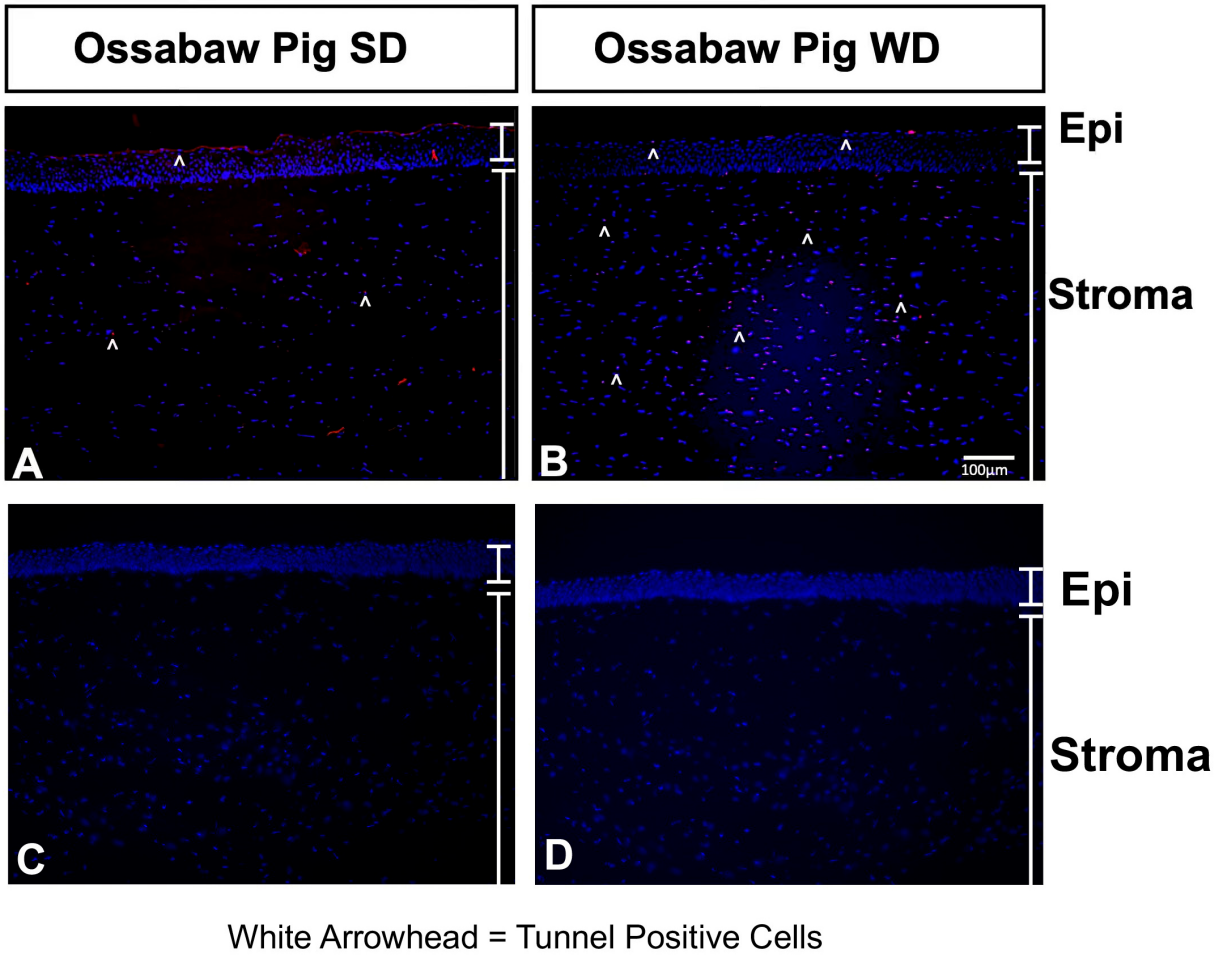

Figure 2. Tunnel assay indicates an increase in Tunnel-positive cells (white arrowheads) in the Western diet (WD) fed Ossabaw mini pigs (**B**) compared to the Standard diet (SD) fed pigs (**A**). Panels **C** and **D** are negative controls where Tdt enzyme and Anti-Digoxigenin Conjugate were respectively excluded during the staining procedure. Arrowheads indicate the apoptotic cells.

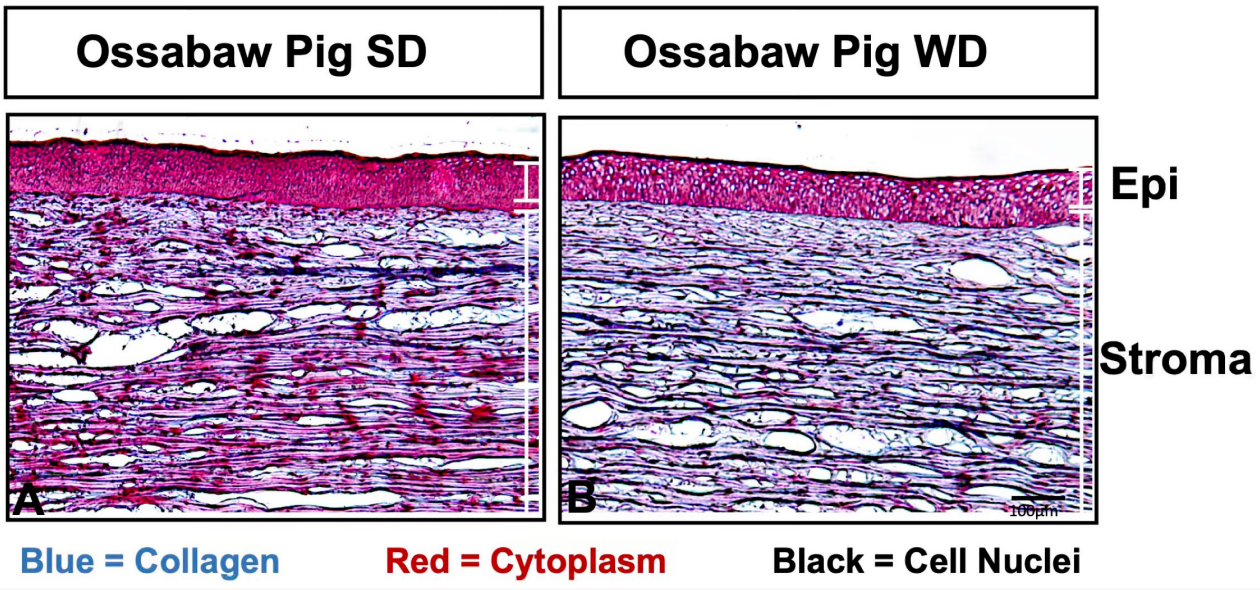

Figure 3. Mason trichome staining depicts cell nuclei (black), cytoplasm (red), and collagens (blue). The Western diet (WD) fed Ossabaw mini pigs (**B**) show decreased cytoplasm staining and a less even blue stain than the Standard diet (SD) fed pigs (**A**).

significantly elevated expression, whereas TGFβ1 was insignificant in the WD group when compared to the SD group (Figure 8B).

DISCUSSION

DM is a multiorgan metabolic syndrome (MetS) marked by uncontrolled hyperglycemia over a prolonged time. In the eye, DR is the most severe disease associated with DM. However, recent clinical studies have described DM, causing significant changes to the cornea, often described as DK [13,15]. Our recent report showed that Ossabaw mini pigs fed on WD for 10 weeks, inducing signs of T2DM and exhibiting neurodegenerative and vascular abnormalities in the retina [33]. Previously, Ossabaw mini pigs have been described as a model for MetS and extensively used for cardiovascular and metabolic disorders [33,45-47]. Also, previous studies have shown that the animal models depicting DM/DR characteristics strongly correlate to the presence of DK [9,13]. Thus, this study is an extension of our previous work concerning diabetic eye diseases. Adding to our previously reported changes in retinal microvasculature, [33] we found that Ossabaw mini pigs showed histological, ultrastructural, and molecular alterations in the corneal stromal collagens when fed on WD.

Histological staining of Ossabaw mini pig corneal tissue sections with H&E showed increased nuclei staining. However, Mason's Trichome staining showed decreased cytoplasm staining accompanied by elevated keratocyte apoptosis in the corneal stroma in the WD-fed group, as observed by the TUNEL staining. These results corroborate that DK might be evident in these keratocytes, causing increased migration of the inflammatory cells toward the anterior stroma and hence the surge in the stromal cell apoptosis, a phenomenon typically seen in the early stages of corneal wound healing. These findings parallel previous studies performed in mice treated with streptozotocin and fed on a high-fat diet. [48,49]

A characteristic arrangement of stromal collagen fibrils in the cornea provides mechanical strength and optical (refractive) power critical for maintaining vision. COL1 is the predominant type of collagen found in the corneal stroma [3]. We investigated histological, molecular, and ultrastructural details of collagen fibrils and arrangement in the corneal stroma of the T2DM and normal mini pig corneas. Histologically, we found that the WD-fed Ossabaw mini pigs showed altered stromal collagen organization. Mason's trichome imaging showed an overall increase in collagen staining supported by the intense immunohistochemical (IHC) staining of COL1 in the stroma of the mini pigs fed on WD. Besides, IHC showed an irregular collagen distribution in WD pigs compared to the SD-fed mini pigs. WD pigs had increased depositions of collagen fibrils throughout the anterior stroma, as observed with Picosirus Red (PSR) staining. We found small bundles of collagen fibrils nearer to

the epithelial-stromal border. This histopathological change parallels a previous study in type 1 diabetic models. [48]

Next, we performed TEM analysis to examine the ultrastructural details of the collagen fibril distribution and arrangement in the stroma of the WD-fed Ossabaw mini pig corneas. TEM imaging and analysis showed a statistical difference in collagen size and distribution. Although WD and SD fed mini pigs have similar smaller-sized collagens (approximately 300 pixels), the larger-sized collagen fibrils decreased from 800 pixels observed in the SD group to 700 pixels in WD pigs, suggesting a role of T2DM in modifying the size of collagen fibrils in the corneal stroma. A previous study by Saito et al. [30] showed the DM decreased collagen quality rather than quantity in bone tissues. We made a similar observation in the corneal stroma in WD pigs. Among the possibilities might be the nascent state of the smaller collagen fibrils in the stroma as seen in the SD group (non-diabetic pigs), which grew continuously in size and maintained a more uniform distance from each other. In contrast, WD pigs predominantly have larger-sized fibrils, which could induce changes in the IFD, as seen in the quantitative analysis of the collagen fibrillar distribution in the cornea. We anticipate that quantitative ultrastructural changes may be insufficient to compromise the vision but may be critical in wound healing after trauma or other pathological states in the eye, such as keratoconus and dry eye. Our TEM findings parallel previous studies, [20,49,50] where they found similar changes in collagen fibrils in diabetic humans and

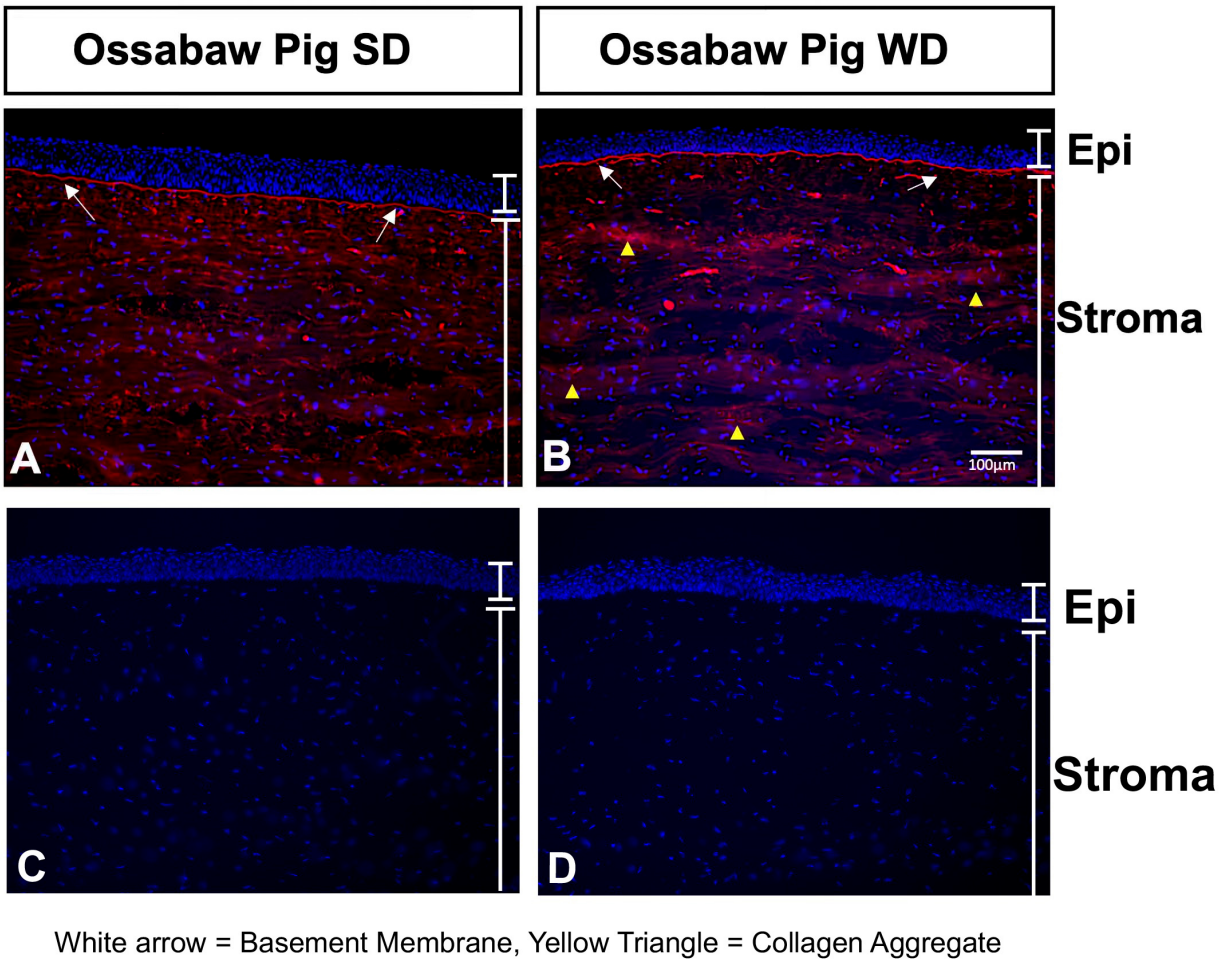

Figure 4. Immunohistochemistry of Collagen I (Col I) displays increased collagen aggregates (yellow triangles) and an increased Col I expression at the basement membrane (white arrows) in the Western diet (WD) fed Ossabaw mini pigs (**B**) compared to the Standard diet (SD) fed pigs (**A**). Panels **C** and **D** are negative controls where primary and secondary antibodies were excluded during antibody staining procedure.

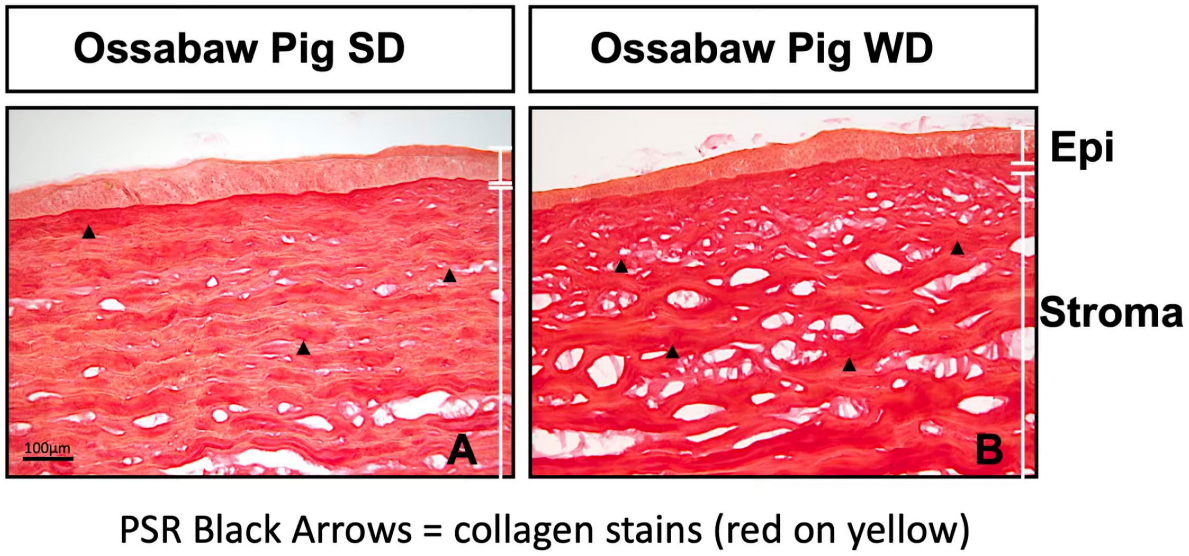

Figure 5. Picrosirius red (PSR) stains collagen in the corneal stroma. A red-on-yellow stain signifies collagen type 1. PSR stained Western diet (WD) fed pig corneal section (**B**) shows high numbers of irregular collagen compared to the Standard diet (SD) fed pigs (**A**).

monkey model [50,51]. However, these studies were limited to a T1DM model.

Adding to histological and ultrastructural findings, we also investigated molecular analysis using real-time qPCR to study the expression pattern of genes concerning the collagen matrix and fibrosis involved in corneal wound healing. Among the predominant concerns in the clinics with diabetic patients is their inability to heal the wounds effectively and promptly [50,52], which prevents them from

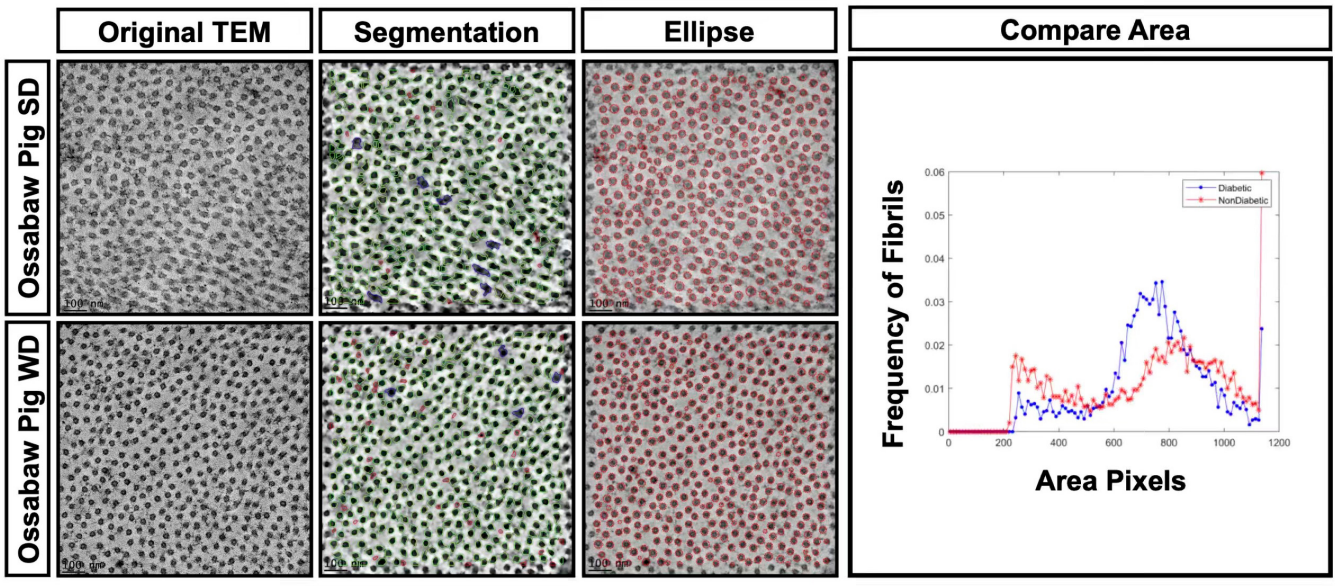

Figure 6. Quantitation of transmission electron microscopy of collagen fibrils in the western diet (WD) fed and Standard diet (SD) fed Ossabaw mini pigs. Panels **A** and **D** are the original transverse section of the transmission electron microscopy images taken at 50,000 magnification. Panels **B** and **F** are segmentations that identify all the collagens present in the figure. Panels **C** and **G** are individual red ellipses made around collagen fibrils used to quantify the size of fibrils. Panel **H** is a graphical representation of collagen fibril sizes found in the image. Western diet pigs show an overall collagen size difference compared to standard diet pigs.

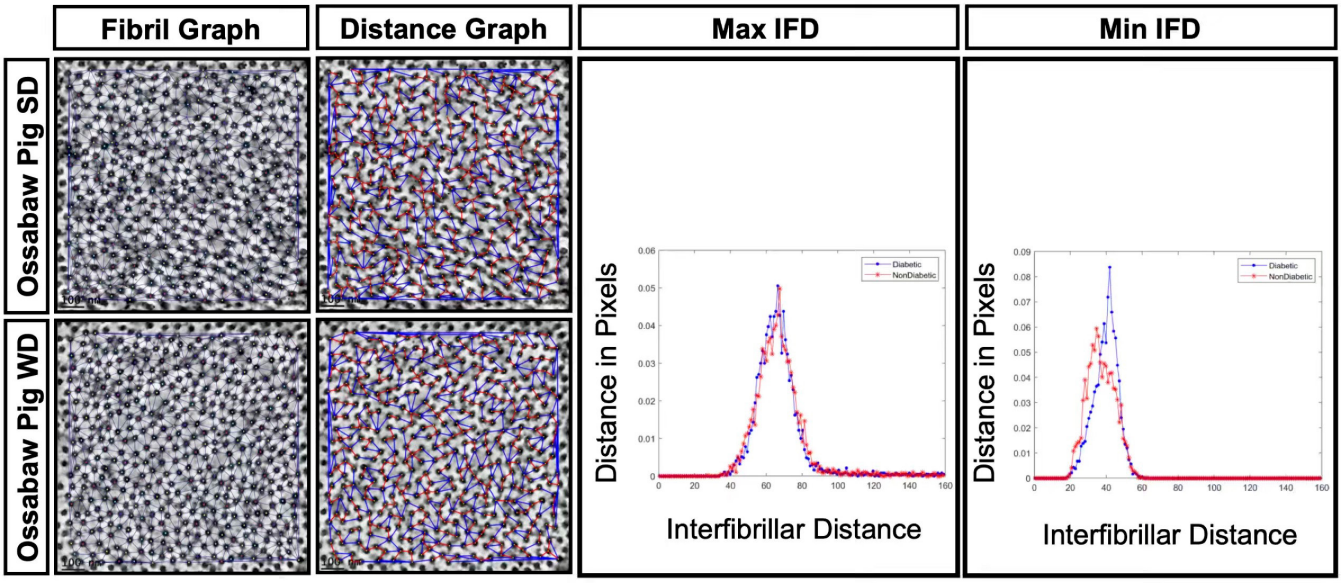

Figure 7. Quantitation of Transmission Electron Microscopy of collagen fibrils in the Western diet (WD) fed and Standard diet (SD) fed Ossabaw mini pigs. **A** and **C** are fibril graphs that show each connection between collagen fibrils. **B** and **D** show the minimum distance between collagen fibrils (red) and the maximum distance between fibrils (blue). **E** is a graphical representation of maximum interfibrillar distance and **F** is a graphical representation of minimum interfibrillar distance.

undergoing ophthalmic procedures, such as refractive surgery or corneal transplants. We found a significant increase in α-SMA and FN, suggesting early fibrotic events in the stroma with increased matrix metalloproteinase 9 (MMP9), a critical extracellular matrix regulatory enzyme. An increase in α-SMA expression parallels a previous study conducted in type 1 diabetic model. [51] Although we found insignificant changes in collage III (COL3), MMP1, or TIMP1 expression, collagen IV (COL4) showed a substantial decline in its expression, depicting the irregularities in the corneal basement membrane of the Ossabaw mini pigs fed on WD. We anticipate that the alterations in the corneal wound healing parameters will result from Ossabaw pigs being fed on WD and developing T2DM.

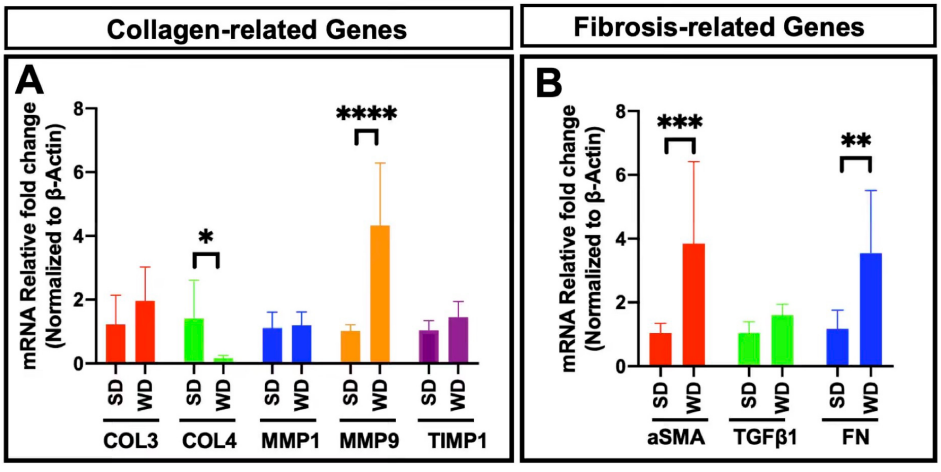

Figure 8. Gene expression in the Western diet (WD) fed and Standard diet (SD) fed Ossabaw pig corneas. **A** represents collagen-related genes- collagen 3 (COL 3), collagen 4 (COL 4), metalloproteases 1 (MMP1), metalloproteases 9 (MMP9), and tissue inhibitor of metalloprotease 1 (TIMP1). **B** represents fibrosis-related genes alpha-smooth muscle action (αSMA), transformation growth factor beta 1 (TGFβ1), and fibronectin (FN). The WD-fed Ossabaw mini pigs corneas had significant alterations in COL4, MMP9, αSMA, TGFβ1, and FN. compared to the SD-fed pigs (P, *<0.05, **<0.01, ***<0.001, ****<0.0001).

In conclusion, Ossabaw mini pigs fed on WD showed histological changes in the stroma, compromised collagen fibrils arrangement, and altered expression of genes involved in corneal wound healing. This pilot study results suggest that corneal stromal wound healing is vulnerable to diabetic conditions and needs further investigation.

ACKNOWLEDGMENTS

The authors thank DeAna G. Grant from the University of Missouri Electron Microscopy Core and Veterinary Medical Diagnostic Laboratory for their help in TEM and histology, respectively. The NIH U42531ODO011140 to NSRRC supported pig facility. This work was supported by the NEI/NIH RO1EY029795 (SSC) and R01EY030774 (RRM) grants and Ruth M Kraeuchi Missouri Endowment of Ophthalmology, University of Missouri Columbia fund (RRM). This investigation was conducted in part in a facility constructed with support from a Research Facilities Improvement Program, grant number C06RR016511 from the National Center for Research Resources, NIH.

REFERENCES

1. Lee SY, Mesfin FB. Blindness. In: *StatPearls*. Elsevier Inc.; 2020. doi:10.1016/B978-0-12-803678-5.00036-910.1016/B978-0-12-803678-5.00036-9
2. Schmidt AM. Highlighting Diabetes Mellitus. Arterioscler Thromb Vasc Biol 2018; 38:e1-8. [PMID: 29282247].
3. Copeland RA, Natalie A. Copeland and Afshari's Principles and Practice of Cornea. 1st edition. Jaypee Brothers Medical Publishers (P) Ltd; 2013. 1460 p.
4. Bullard KM, Cowie CC, Lessem SE, Saydah SH, Menke A, Geiss LS, Orchard TJ, Rolka DB, Imperatore G. Prevalence of Diagnosed Diabetes in Adults by Diabetes Type — United States, 2016. MMWR Morb Mortal Wkly Rep 2018; 67:359-61. [PMID: 29596402].
5. Negi A, Vernon SA. An overview of the eye in diabetes. In: *Journal of the Royal Society of Medicine*. Vol 96. Royal Society of Medicine Press Ltd; 2003:266–272. doi:10.1258/jrsm.96.6.26610.1258/jrsm.96.6.266
6. Cabrera AP, Mankad RN, Marek L, Das R, Rangasamy S, Monickaraj F, Das A. Genotypes and phenotypes: A search for influential genes in diabetic retinopathy. Int J Mol Sci 2020; 21:[PMID: 32295293].
7. Karagöz IK, Allahverdiyev A, Bağlrova M, Abamor ES, Dinparvar S. Current Approaches in Treatment of Diabetic Retinopathy and Future Perspectives. J Ocul Pharmacol Ther 2020; 36:487-96. [PMID: 32453671].
8. Priyadarsini S, Whelchel A, Nicholas S, Sharif R, Riaz K, Karamichos D. Diabetic keratopathy: Insights and challenges. Surv Ophthalmol 2020; 65:513-29. [PMID: 32092364].
9. Ljubimov AV. Diabetic complications in the cornea. Vision Res 2017; 139:138-52. [PMID: 28404521].
10. Goldstein AS, Janson BJ, Skeie JM, Ling JJ, Greiner MA. The effects of diabetes mellitus on the corneal endothelium: A review. Surv Ophthalmol 2020; 65:438-50. [PMID: 31926185].
11. Lass JH, Benetz BA, Patel SV, Szozotka-Flynn L. O'Brien, Ayala AR, Maguire MG, Daoud YJ, Greiner MA, Hannush SB, Lee WB, Mauger TF, Menegay HJ, Mifflin MD, Raizman MB, Rose-Nussbaumer J, Schultze RL, Schmidt GA, Sugar A, Terry MA, Verdier DD, Cornea Preservation Time Study Group. Donor, Recipient, and Operative Factors Associated with Increased Endothelial Cell Loss in the Cornea Preservation Time Study. JAMA Ophthalmol 2019; 137:185-93. [PMID: 30422157].
12. Wang B, Yang S, Zhai HL, Zhang YY, Cui CX, Wang JY, Xie LX. A comparative study of risk factors for corneal infection in diabetic and non-diabetic patients. Int J Ophthalmol 2018; 11:43-7. [PMID: 29375989].
13. Zhao H, He Y, Ren YR, Chen BH. Corneal alteration and pathogenesis in diabetes mellitus. Int J Ophthalmol 2019; 12:1939-50. [PMID: 31850180].
14. Han SB, Yang HK, Hyon JY. Influence of diabetes mellitus on anterior segment of the eye. Clin Interv Aging 2018; 14:53-63. [PMID: 30643394].
15. Mansoor H, Tan HC, Tzu-Yun Lin M, Mehta JS, Liu YC. Diabetic corneal neuropathy. J Clin Med 2020; 9:3956-[PMID: 33291308].
16. Shah R, Amador C, Tormanen K, Ghiam S, Saghizadeh M, Arumugaswami V, Kumar A, Kramerov AA, Ljubimov AV. Systemic diseases and the cornea. Exp Eye Res 2021; 204:108455-[PMID: 33485845].
17. Bikbova G, Oshitari T, Baba T, Bikbov M, Yamamoto S. Diabetic corneal neuropathy: Clinical perspectives. Clin Ophthalmol 2018; 12:981-7. [PMID: 29872257].
18. Kalteniece A, Ferdousi M, Azmi S, Marshall A, Soran H, Malik RA. Keratocyte density is reduced and related to corneal nerve damage in diabetic neuropathy. Invest Ophthalmol Vis Sci 2018; 59:3584-90. [PMID: 30025082].
19. Priyadarsini S, McKay TB, Sarker-Nag A, Allegood J, Chalfant C, Ma JX, Karamichos D. Complete metabolome and lipidome analysis reveals novel biomarkers in the human diabetic corneal stroma. Exp Eye Res 2016; 153:90-100. [PMID: 27742548].
20. Del Buey MA, Casas P, Caramello C, Lopez N, de la Rica M, Subiron AB, Lanchares E, Huerva V, Grzybowski A, Ascaso FJ. An Update on Corneal Biomechanics and Architecture in Diabetes. J Ophthalmol 2019; 2019:[PMID: 31275634].
21. Sady C, Khosrof S, Nagaraj R. Advanced Maillard Reaction and Crosslinking of Corneal Collagen in Diabetes. Biochem Biophys Res Commun 1995; 214:793-7. [PMID: 7575546].
22. Rehany U, Ishii Y, Lahav M, Rumelt S. Ultrastructural changes in corneas of diabetic patients: An electron- microscopy study. Cornea 2000; 19:534-8. [PMID: 10928773].

23. Zou C, Wang S, Huang F, Zhang YA. Advanced Glycation End Products and Ultrastructural Changes in Corneas of Long-term Streptozotocin-Induced Diabetic Monkeys. Cornea 2012; 31:1455-9. [PMID: 22695699].

24. Meek KM, Tuft SJ, Huang Y, Gill PS, Hayes S, Newton RH, Bron AJ. Changes in collagen orientation and distribution in keratoconus corneas. Invest Ophthalmol Vis Sci 2005; 46:1948-56. [PMID: 15914608].

25. Meek KM. Corneal collagen-its role in maintaining corneal shape and transparency. Biophys Rev 2009; 1:83-93. [PMID: 28509987].

26. Meek KM, Knupp C. Corneal structure and transparency. Prog Retin Eye Res 2015; 49:1-16. [PMID: 26145225].

27. Michelacci YM. Collagens and proteoglycans of the corneal extracellular matrix. Braz J Med Biol Res 2003; 36:1037-46. [PMID: 12886457].

28. Ravelojaona V, Robert AM, Robert L, Renard G. Collagen biosynthesis in cell culture: Comparison of corneal keratocytes and skin fibroblasts. Effect of rhamnose-rich oligo- and polysaccharides. Pathol Biol (Paris) 2008; 56:66-9. [PMID: 18178024].

29. Zyablitskaya M, Jayyosi C, Takaoka A, Myers KM, Suh LH, Nagasaki T, Trokel SL, Paik DC. Topical corneal cross-linking solution delivered via corneal reservoir in Dutch-belted rabbits. Transl Vis Sci Technol 2020; 9:1-12. [PMID: 32879776].

30. Saito M, Kida Y, Kato S, Marumo K. Diabetes, collagen, and bone quality. Curr Osteoporos Rep 2014; 12:181-8. [PMID: 24623537].

31. Sturek M, Alloosh M, Wenzel J, Byrd JP, Edwards JM, Lloyd PG, Tune JD, March KL, Miller MA, Mokelke EA, Brisbin IL. Ossabaw Island miniature swine: Cardiometabolic syndrome assessment. In Swine in the Laboratory: Surgery, Anesthesia, Imaging, and Experimental Techniques, Second Edition. 2007. CRC Press. pp. 397-402.

32. Dyson MC, Alloosh M, Vuchetich JP, Mokelke EA, Sturek M. Components of Metabolic Syndrome and Coronary Artery Disease in Female Ossabaw Swine Fed Excess Atherogenic Diet. Comp Med 2006; 56:35-45. [PMID: 16521858].

33. Lim RR, Grant DG, Olver TD, Padilla J, Czajkowski AM, Schnurbusch TA, Mohan RR, Hainsworth DP, Walters EM, Chaurasia SS. Young ossabaw pigs fed a western diet exhibit early signs of diabetic retinopathy. Invest Ophthalmol Vis Sci 2018; 59:2325-38. [PMID: 29847637].

34. Vieira-Potter VJ, Karamichos D, Lee DJ. Ocular Complications of Diabetes and Therapeutic Approaches. BioMed Res Int 2016; 2016:[PMID: 27119078].

35. Tandon A, Tovey JCK, Waggoner MR, Sharma A, Cowden JW, Gibson DJ, Liu Y, Schultz GS, Mohan RR. Vorinostat: A potent agent to prevent and treat laser-induced corneal haze. J Refract Surg 2012; 28:285-90. [PMID: 22386369].

36. Tandon A, Sharma A, Rodier JT, Klibanov AM, Rieger FG, Mohan RR. BMP7 Gene Transfer via Gold Nanoparticles into Stroma Inhibits Corneal Fibrosis In Vivo. PLoS One 2013; 8:1-9. [PMID: 23799103].

37. Mohan RR, Tovey JCK, Sharma A, Schultz GS, Cowden JW, Tandon A. Targeted decorin gene therapy delivered with adeno-associated virus effectively retards corneal neovascularization in vivo. PLoS One 2011; 6:[PMID: 22039486].

38. Gronkiewicz KM, Giuliano EA, Kuroki K, Bunyak F, Sharma A, Teixeira LBC, Hamm CW, Mohan RR. Development of a novel in vivo corneal fibrosis model in the dog. Exp Eye Res 2016; 143:75-88. [PMID: 26450656].

39. Ersoy I, Bunyak F, Higgins JM, Palaniappan K. Coupled edge profile active contours for red blood cell flow analysis. 2012 9th IEEE International Symposium on Biomedical Imaging (ISBI), 2012, pp. 748-751.

40. Sun M, Huang J, Bunyak F, Gumpper K, De G, Sermersheim M, Liu G, Lin PH, Palaniappan K, Ma J. Superresolution microscope image reconstruction by spatiotemporal object decomposition and association: application in resolving t-tubule structure in skeletal muscle. Opt Express 2014; 22:12160-[PMID: 24921337].

41. Vincent L, Vincent L, Soille P. Watersheds in Digital Spaces: An Efficient Algorithm Based on Immersion Simulations. IEEE Trans Pattern Anal Mach Intell 1991; 13:583-98. .

42. Soille P. *Morphological Image Analysis*. Springer Berlin Heidelberg; 1999.

43. Nath SK, Palaniappan K, Bunyak F. Cell segmentation using coupled level sets and graph-vertex coloring. *Med Image Comput Comput Assist Interv*. 2006;9(Pt 1):101–108.

44. Gupta S, Fink MK, Ghosh A, Tripathi R, Sinha PR, Sharma A, Hesemann NP, Chaurasia SS, Giuliano EA, Mohan RR. Novel combination BMP7 and HGF gene therapy instigates selective myofibroblast apoptosis and reduces corneal haze in vivo. Invest Ophthalmol Vis Sci 2018; 59:1045-57. [PMID: 29490341].

45. Neeb ZP, Edwards JM, Alloosh M, Long X, Mokelke EA, Sturek M. Metabolic syndrome and coronary artery disease in ossabaw compared with yucatan swine. Comp Med 2010; 60:300-15. [PMID: 20819380].

46. Olijhoek J. The Metabolic Syndrome is associated with advanced vascular damage in patients with coronary heart disease, stroke, peripheral arterial disease or abdominal aortic aneurysm. Eur Heart J 2004; 25:342-8. [PMID: 14984924].

47. Olver TD, Grunewald ZI, Jurrissen TJ, MacPherson REK, LeBlanc PJ, Schnurbusch TR, Czajkowski AM, Laughlin MH, Rector RS, Bender SB, Walters EM, Emter CA, Padilla J. Microvascular insulin resistance in skeletal muscle and brain occurs early in the development of juvenile obesity in pigs. Am J Physiol Regul Integr Comp Physiol 2018; 314:R252-64. [PMID: 29141949].

48. Markoulli M, Flanagan J, Tummanapalli SS, Wu J, Willcox M. The impact of diabetes on corneal nerve morphology and ocular surface integrity. Ocul Surf 2018; 16:45-57. [PMID: 29113918].

49. Bikbova G, Oshitari T, Tawada A, Yamamoto S. Corneal Changes in Diabetes Mellitus. Curr Diabetes Rev 2012; 8:294-302. [PMID: 22587515].

50. Bu Y, Shih KC, Kwok SS, Chan YK, Cheuk-Yin Lo A, Chan TCY, Jhanji V, Tong L. Experimental modeling of cornea wound healing in diabetes: Clinical applications and beyond. BMJ Open Diabetes Res Care 2019; 7:779-[PMID: 31803484].

51. McKay TB, Priyadarsini S, Karamichos D. Mechanisms of Collagen Crosslinking in Diabetes and Keratoconus. Cells 2019; 8:1-28. [PMID: 31614631].

52. Maruyama K, Asai J, Ii M, Thorne T, Losordo DW, D'Amore PA. Decreased macrophage number and activation lead to reduced lymphatic vessel formation and contribute to impaired diabetic wound healing. Am J Pathol 2007; 170:1178-91. [PMID: 17392158].

Articles are provided courtesy of Emory University and the Zhongshan Ophthalmic Center, Sun Yat-sen University, P.R. China. The print version of this article was created on 7 December 2021. This reflects all typographical corrections and errata to the article through that date. Details of any changes may be found in the online version of the article.